State-selective electron transfer in $He^+ + He$ collisions at intermediate energies

J. W. Gao,[1,2,*] Y. Wu,[1,3] J. G. Wang,[1] N. Sisourat,[2] and A. Dubois[2]
[1]*Institute of Applied Physics and Computational Mathematics, 100088 Beijing, China*
[2]*Sorbonne Université, CNRS, Laboratoire de Chimie Physique-Matière et Rayonnement, F-75005 Paris, France*
[3]*HEDPS, Center for Applied Physics and Technology, Peking University, 100084 Beijing, China*

(Received 20 February 2018; published 21 May 2018)

Electron transfer processes in $He^+ + He$ collisions are studied theoretically using a three-electron semiclassical atomic-orbital close-coupling method in a wide energy domain, from 1 to 225 keV/u. Total, state-selective, and angular-differential cross sections are presented and compared with available experimental and theoretical results. A prominent oscillatory energy dependence structure in the transfer-excitation cross sections is observed and explained by a strong competition between these channels and the projectile-excitation processes. Moreover, the angular-differential cross sections considered in this work exhibit an oscillatory structure which is interpreted within a Fraunhofer-type diffraction model. For the two highest considered collision energies, the cross sections show a different pattern for which both Fraunhofer-type diffraction and the Thomas mechanism have to be advocated.

DOI: 10.1103/PhysRevA.97.052709

I. INTRODUCTION

Experimentally, $He^+ + He$ collisions have received a great deal of interest for several decades up to very recently [1–12]. Most of the early works focused on the total and state-selective cross sections, which do not provide as much information on the collision dynamics as the differential scattering cross sections. However, in recent works, the ground-state transfer angular-differential cross sections in $^3He^+ + {}^4He$ collisions have been measured by Schöffler *et al.* [11] at 60, 150, 300, and 600 keV/u impact energies using the cold-target recoil-ion-momentum spectroscopy (COLTRIMS) technique. The authors have also shown the corresponding cross sections using the four-body distorted-wave theory. A rather poor agreement was found between the calculations and their experimental measurements. On the other hand, Guo *et al.* [12] performed a combined experimental and theoretical investigation on state-selective and angular-differential cross sections in $^4He^+ + {}^4He$ collisions. The cross sections were obtained experimentally using the COLTRIMS technique at 7.5 and 25 keV/u impact energies. The experimental data were compared with the theoretical results based on the classical trajectory Monte Carlo (CTMC) method. It was found that the CTMC calculations failed to reproduce the experimental angular-differential cross sections.

Despite the substantial number of theoretical efforts that have been pursued to understand and model the $He^+ + He$ collision system [13–21], this latter still remains a challenge for theoreticians. In particular, in the intermediate impact energy region, perturbative approaches or model calculations using a model potential with only one (or two) active electrons may be inadequate due to the strong coupling between various channels and electronic correlation effects. Consequently, nonperturbative full three-electron semiclassical or quantum approaches can bring further insights into the understanding of this collision system.

In this context, Sural *et al.* [17] developed in 1969 a three-electron coupled-channel method to study electron transfer and excitation processes of $He^+ + He$ collisions for the impact energies 0.15–10 keV/u; the authors considered only six channels which allowed for a single excitation and transfer into the first excited states. But direct projectile excitation was excluded. Later, extended three-electron coupled-channel calculations were performed for the impact energies 2.5–150 keV/u by Hildenbrand *et al.* [18], where 128 channels were considered in their calculations. However, the couplings between s and p wave functions were not taken into account in their calculations. It should be also mentioned that those studies were only focused on the total state-selective cross sections.

In the present paper, we study theoretically the electron transfer processes

$$\begin{aligned} He^+(1s) + He(1s^2) &\rightarrow He(1s^2) + He^+(1s) \quad \text{(GT)}, \\ &\rightarrow He(1snl) + He^+(1s) \quad \text{(ET)}, \\ &\rightarrow He(1s^2) + He^+(nl) \quad \text{(TE)}, \end{aligned} \tag{1}$$

where GT, ET, and TE correspond to ground-state transfer, transfer to excited state, and transfer-excitation, respectively. We use a three-electron semiclassical atomic-orbital close-coupling (SCAOCC) method and focus in the energy domain ranging from 1 to 225 keV/u. Total, state-selective, and angular-differential cross sections are presented and compared with available theoretical and experimental results. Our computed cross sections agree well with the most recent experimental measurements. Possible reasons for the disagreement with previous calculations are discussed. Furthermore, our calculations show a prominent oscillatory energy dependence structure in the integral TE cross sections, which we assign to a strong competition between the TE and projectile-excitation processes. The angular-differential cross sections for most

*junwen.gao@etu.upmc.fr

processes considered in this work exhibit distinct oscillatory structures which are discussed and interpreted.

The present paper is organized as follows. In the next section we briefly outline our three-electron SCAOCC method used in the present calculations. Section III is devoted to the detailed analysis of the total, state-selective, and angular-differential cross sections and direct comparisons with available experimental and theoretical results, followed by the conclusions in Sec. IV. Atomic units are used throughout, unless explicitly indicated otherwise.

II. THEORY

In the present work, the cross sections of the electronic processes in Eq. (1) occurring during $He^+ + He$ collisions are calculated by a three-electron semiclassical atomic-orbital close-coupling approach. We have previously described our multiple (two)-active-electron SCAOCC approach in, e.g., [22–24], so only the main features of the approach are outlined here. The n_e-electron time-dependent Schrödinger equation (TDSE) is written as

$$\left[H_e - i\frac{\partial}{\partial t}\bigg|_{\vec{r}_1,\vec{r}_2,\ldots,\vec{r}_{n_e}}\right]\Psi(\vec{r}_1,\vec{r}_2,\ldots,\vec{r}_{n_e},\vec{R}(t)) = 0, \quad (2)$$

where H_e is the electronic Hamiltonian,

$$H_e = \sum_{i=1,n_e}\left(-\frac{1}{2}\nabla_i^2 + V_T(r_i) + V_P(r_i^p) + \sum_{i<j}\frac{1}{|\vec{r}_i - \vec{r}_j|}\right), \quad (3)$$

and $\vec{r}_i, \vec{r}_i{}^p = \vec{r}_i - \vec{R}(t)$ are the position vectors of the electrons with respect to the target and the projectile, respectively. The relative projectile-target position $\vec{R}(t)$ defines the trajectory, with $\vec{R}(t) = \vec{b} + \vec{v}t$ in the usual straight-line, constant-velocity approximation ($\vec{b}$ and $\vec{v}$ are the impact parameter and velocity, see Fig. 1.). The term V_T (V_P) is the electron-target (-projectile) nucleus potential.

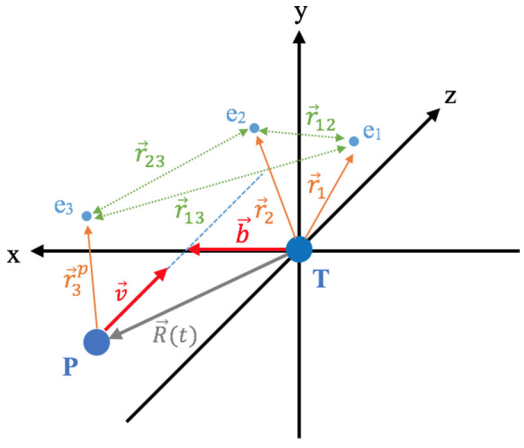

FIG. 1. Collision geometry. The impact parameter $\vec{b}$ and velocity $\vec{v}$ define the collision plane (xz) and $\vec{R}(t)$ the projectile (P) trajectory with respect to the target (T). The positions of first two electrons with respect to the target center are denoted $\vec{r}_1$, $\vec{r}_2$, the third electron with respect to the projectile center is denoted $\vec{r}_3^{\,p}$, and $\vec{r}_{12}$, $\vec{r}_{13}$ and $\vec{r}_{23}$ are the relative vectors between every two electrons. Note that for clarity we locate the origin of the reference on the target; this does not restrict the generality of our results which are Galilean invariant.

The Schrödinger equation is solved by expanding the wave function onto a basis set composed of states of the isolated collision partners,

$$\Psi(\vec{r}_1,\vec{r}_2,\ldots,\vec{r}_{n_e},\vec{R}(t)) = \sum_{n_T,n_P}\sum_{J=1}^{N_{(n_T,n_P)}}\Big[a_J^{(n_T,n_P)}(t) \times \Phi_J^{(n_T,n_P)}(\vec{r}_1,\vec{r}_2,\ldots,\vec{r}_{n_e},\vec{R}(t))\, e^{-iE_J^{(n_T,n_P)}t}\Big], \quad (4)$$

with

$$\Phi_{J\equiv(j_T,j_P)}^{(n_T,n_P)}(\vec{r}_1,\vec{r}_2,\ldots,\vec{r}_{n_e},\vec{R}(t)) = \hat{\mathbb{P}}\Big[\phi_{j_T}^{T_{n_T}}(\vec{r}_1,\vec{r}_2,\ldots,\vec{r}_{n_T}) \times \phi_{j_P}^{P_{n_P}}(\vec{r}_{n_T+1}^{\,p},\vec{r}_{n_T+2}^{\,p},\ldots,\vec{r}_{n_T+n_P}^{\,p})\Big], \quad (5)$$

where $N_{(n_T,n_P)}$ denotes the number of states (and corresponding energies) for which n_T and n_P ($n_T + n_P = n_e$) electrons are on the target and projectile, respectively. The multielectron states $\Phi^{(n_T,n_P)}$ are expressed as linear combinations of spin-adapted products of Gaussian-type orbitals (GTOs) centered on isolated collision partners. The permutation operator $\hat{\mathbb{P}}$ in Eq. (5) ensures the full antisymmetry of the wave functions with respect to the interchange of two electrons. Note that, for all electrons, these projectile states contain plane-wave electron translation factors (ETFs), $e^{i\vec{v}\cdot\vec{r}-i\frac{1}{2}v^2t}$, ensuring Galilean invariance of the results. The insertion of Eqs. (4) and (5) into Eq. (3) results in a system of first-order coupled differential equations, which can be written in matrix form as

$$i\frac{d}{dt}\mathbf{a}(t) = \mathbf{S}^{-1}(\vec{b},\vec{v},t)\mathbf{M}(\vec{b},\vec{v},t)\mathbf{a}(t), \quad (6)$$

where $\mathbf{a}(t)$ is the column vector of the time-dependent expansion coefficients and $\mathbf{S}$, $\mathbf{M}$ are the overlap and coupling matrices, respectively. These equations are solved for a set of initial conditions (initial state i, b, and v) using a robust predictor-corrector time-step variable method developed by Shampine and Gordon [25]. The probability of a transition $i \to f$ is given by the coefficients a_f ($\equiv a_J^{(n_T,n_P)}$) as

$$P_{fi}(b,v) = \lim_{t\to\infty}|a_f(t)|^2. \quad (7)$$

The corresponding integral (total) cross sections for the considered transition are calculated as

$$\sigma_{fi}(v) = 2\pi\int_0^{+\infty} bP_{fi}(b,v)db. \quad (8)$$

In the same manner as in Ref. [26], the angular-differential cross sections are expressed by

$$\frac{d\sigma_{fi}}{d\Omega} = |f_{fi}(\theta,\phi)|^2, \quad (9)$$

where the scattering amplitude is given as a Bessel function transform of the collision amplitude,

$$f_{fi}(\theta,\phi) = \mu v(-i)^{1+|m_f-m_i|}e^{-i(m_f-m_i)\phi} \times \int_0^{\infty} bdbJ_{|m_f-m_i|}[2\mu vb\sin(\theta/2)] \times [c_{fi}(b,+\infty) - \delta_{fi}], \quad (10)$$

where μ is the reduced mass of the target and projectile and m_i, m_f are the magnetic quantum numbers of the initial and final states, respectively. It should be noted that all b-dependent phases (i.e., common phases due to the core-core interaction in the Hamiltonian [27]) contributing to the collision amplitudes $c_{fi}(b,+\infty)$ in the complete solution of the close-coupled impact parameter equations should be included in Eq. (10). It is precisely the complete phase information that allows the extraction of the angular predictions from straight-line trajectory collision amplitudes. Explicitly, the amplitudes are

$$c_{fi}(b,+\infty) = a_f(b,Z_0)\exp\left(\frac{i}{v}2Z^T Z^P \ln b\right), \qquad (11)$$

where the nuclear charges of the target and projectile are denoted as Z^T and Z^P, the amplitude $a_f(b,Z_0)$ is the solution of Eq. (6), starting (initial conditions) at $-Z_0$ along the projectile trajectory and ending at $+Z_0$, for the usual left-side passage of the target ($\phi = 0$, cf. Fig. 1 in [26]).

III. RESULTS AND DISCUSSION

A. Total and state-selective cross sections

In the present calculations, a set of 19 GTOs (10 for $l = 0$, 3×3 for $l = 1$) are used on both projectile and target centers; this allows the inclusion of 1260 states (states of two electrons on target and one electron on projectile, and vice-versa). Note that this basis has been selected using two criteria: (i) large enough to describe accurately the important target and projectile states and (ii) still computationally tractable. Convergence tests have been performed by comparing the present results with those from a smaller basis set (12 GTOs on each center, i.e., 6 for $l = 0$ and 2×3 for $l = 1$) which allows the inclusion of 582 states in total. The convergence was evaluated to be better than 1% for the total single electron transfer (SET) and GT cross sections, to be about 10% for the ET cross sections, reaching a maximum of 20% for the TE cross sections, for energies where, however, the values of the cross sections are lower than 5×10^{-18} cm^2 (see Fig. 3).

In Fig. 2, our calculated total SET cross sections are presented and compared with experimental data [1,4,7,9,10] and theoretical calculations [12,14,20], as well as the recommended data from Ref. [28]. As displayed in Fig. 2, our results are in very good agreement with experimental measurements and the four-body Coulomb-Born distorted-wave approximation (CBDW-4B) calculations [14] in the whole overlapping energy region. The cross sections from the time-dependent-density-functional-theory (TDDFT) calculations of Baxter *et al.* [20] are higher than our results. In particular, for $E > 50$ keV/u, the TDDFT calculations overestimate the cross sections compared to the experimental data; this failure may be related to the fact that the authors employed an independent electron model (IEM) approximation in their calculations [20]. This indicates that the correlation effects which have been taken into account in the present calculations as well as in the CBDW-4B calculations [14] are most important for impact energies 50–225 keV/u (the highest impact energy we considered). It can also be observed from Fig. 2 that the CTMC calculations of Guo *et al.* [12] lie below our results and the CBDW-4B calculations [14], as well as the experimental

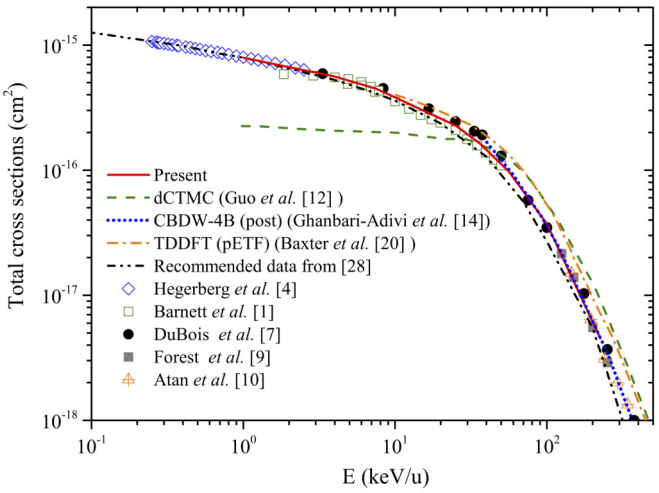

FIG. 2. Total SET cross sections as a function of impact energy. The theoretical results are from the present calculations (red solid line), Guo *et al.* [12] (green dash line), Ghanbari-Adivi *et al.* [14] (blue dot line), and Baxter *et al.* [20] (orange dash-dot line). The experimental results are from Hegerberg *et al.* [4] (blue open diamonds), Barnett *et al.* [1] (green open squares), DuBois *et al.* [7] (black solid circles), Forest *et al.* [9] (grey solid squares), and Atan *et al.* [10] (orange crossed triangles). The recommended data from [28] (black dash-dot-dot line) are also presented.

measurements for the impact energies lower than 30 keV/u, while slightly above for the impact energies above 50 keV/u. This could be due to the fact that the interelectronic interactions were taken into account by an approximate way and because of the lack of the tunneling effect in their CTMC method [12]. Note, finally, that the data from Ref. [28] are also in good agreement with measurements of [1,4] for $E < 3$ keV, but are slightly lower than [7,9,10] for higher impact energies.

The total state-selective (GT, ET, and TE) cross sections as functions of the impact energy are shown in Fig. 3(a), together with experimental and theoretical results of Guo *et al.* [12] for comparison. Our results show that the GT process in Fig. 3(a) is the dominant channel in the entire energy range with an increase for decreasing impact energies, which is a general feature for the resonant charge-transfer process in a symmetric ion-atom collision system.

In contrast to the GT process, the cross sections of ET show a maximum around 25 keV/u, and a monotonous decrease at both higher and lower energies. It can also be observed from Fig. 3(a) that the electron transfer to He excited triplet states are the dominant contributions of the ET cross sections. For $E >$ 70 keV/u, the ratio of ET to triplet and singlet states is about 3, which is in accordance with straightforward spin statistics. This indicates that it is a direct atomic mechanism which gives rise to the process in this energy range while for $E < 70$ keV/u one can advocate a complex dynamics, coupling a molecular type mechanism and the direct one. Comparing with experimental results of Guo *et al.* [12], very good agreements can be observed for both GT and ET cross sections.

For the TE cross sections, our results are slightly larger and smaller than the experimental data [12] at, respectively, $E = 7.5$ and $E = 25$ keV/u. It should be noted that these

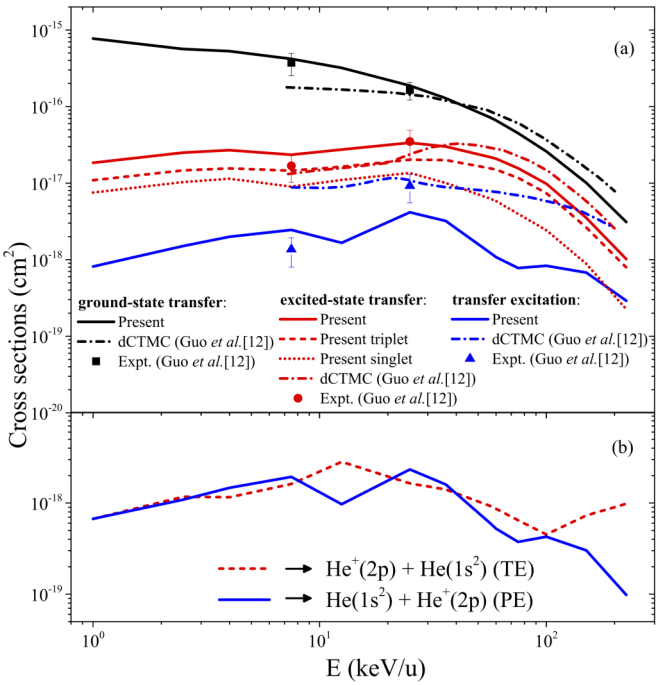

FIG. 3. GT, ET, and TE cross sections as functions of impact energy for $He^+ + He$ collisions. (a) Solid line: present calculations; the present calculated cross sections for ET to singlet and triplet states of He are denoted as red dot and dash line, respectively; dash-dot line: theoretical calculations of [12]; solid symbols: experimental measurements of [12]. (b) Our calculated cross sections for the dominant TE and PE processes as functions of impact energy.

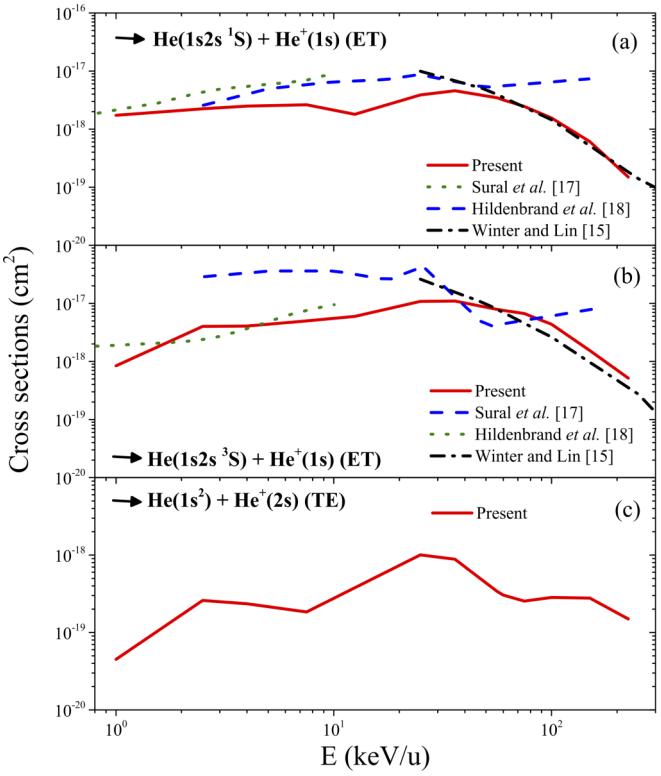

FIG. 4. Cross sections as functions of impact energy for ET to $He(1s2s\ ^1S$ and $^3S)$ excited states and TE to the $He^+(2s)$ excited state.

cross sections are small and our calculations are less converged (20%) than for the other processes. However, the tendency of our results are in accordance with the data of [12]. In contrast, the CTMC calculations reported in [12] are much larger than their experimental data at 7.5 keV/u, and show a very weak dependence upon impact energy in the range considered. In absence of other independent results, it is difficult to draw definite conclusions on that disagreement. However, for the different processes considered, our results show the best overall agreement with experimental results.

Furthermore, it can be seen in Fig. 3(a) that our calculated TE cross sections show a clear oscillatory dependence structure as a function of impact energy. To gain insight into the oscillatory structure, we present in Fig. 3(b) the cross sections for the dominant channels of two symmetric processes,

$$\begin{aligned} He^+(1s) + He(1s^2) &\rightarrow He(1s^2) + He^+(2p) \quad (TE), \\ &\rightarrow He^+(2p) + He(1s^2) \quad (PE), \end{aligned} \tag{12}$$

where PE stands for projectile excitation. It can be observed that the TE and PE cross sections seem to be out of phase over the energy range 3–225 keV/u, demonstrating the existence of the strong competition between TE and PE resonant processes. However, there exist only two experimental data for the TE process [12], and further experimental measurements will be useful to confirm our theoretical predicted oscillatory structure.

As shown above, our calculations agree quantitatively with the most recent measurements of Guo *et al.* [12]. In the following, we further investigate electron transfer processes for which no recent theoretical and experimental results are available.

The cross sections for ET to $He(1s2s\ ^1S$ and $^3S)$ excited states and TE to $He^+(2s)$ excited state are presented respectively in Fig. 4(a)–4(c). The theoretical results of Sural *et al.* [17], Winter *et al.* [15], and Hildenbrand *et al.* [18] are also reported. To our knowledge, no experimental results are available. It can be seen for both electron transfer to $He(1s2s\ ^1S)$ and $He(1s2s\ ^3S)$, large discrepancies exist among all these theoretical results in the overlapping energy regions and a surprising very good agreement with first-Born calculations [15] is found for the first process at $E > 50$ keV/u. For the cross sections of TE in Fig. 4(c), a prominent oscillatory structure can be observed, which is due to the strong competition between TE and PE processes, as mentioned before for total TE cross sections. However, to our knowledge, no experimental or theoretical investigations exist to confirm our predictions.

The convergence of our calculations has been checked for the three processes under consideration, as mentioned before. The validity of our results is also supported by the comparison with experiments concerning electron transfer to higher $He(1s2p\ ^1P, 1s3s\ ^1S$ and $^3S)$ excited states. We present in Fig. 8 (see the Appendix) our calculated cross sections for electron transfer to $He(1s2p\ ^1P, 1s3s\ ^1S$ and $^3S)$ excited states, compared with available experimental and theoretical results [8,15,18,29,30]. Our results are in excellent agreement with the experimental results of [8,29,30] in the overlapping energy regions. The validity of our calculated cross sections for ET to $He(1s2s\ ^1S$ and $^3S)$ excited states and TE to the

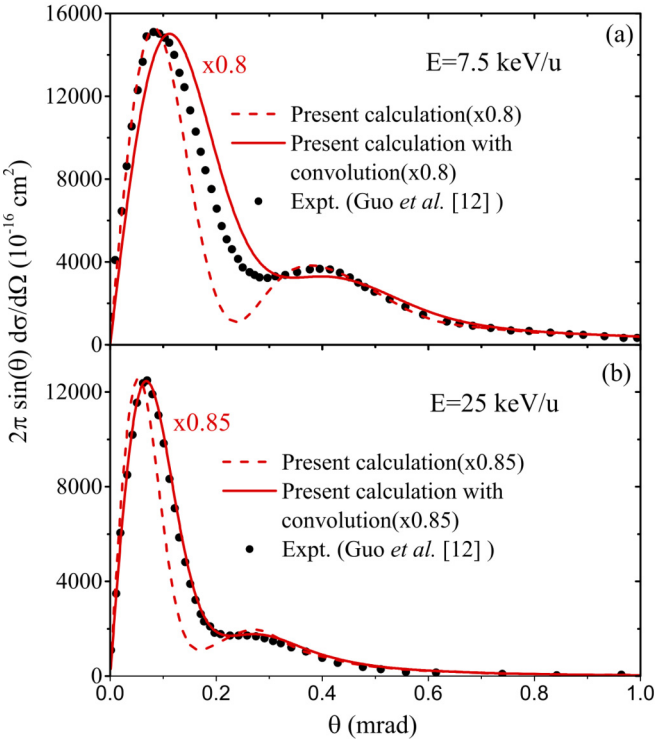

FIG. 5. GT angular-differential cross sections as a function of scattering angle at impact energies 7.5 and 25 keV/u. Red solid line: present calculations; red dash line: present convoluted results; black solid circles: experimental results from [12].

$He^{+}(2s)$ excited state in Fig. 4 is supported by this agreement, since the lower excited states are obviously better described than the higher excited states with our GTO basis set. Further experimental investigations will be useful to draw definite conclusions.

B. Angular-differential cross sections

We now investigate the electron transfer angular-differential cross sections which provide a greater benchmark for our calculations. In Fig. 5, our calculated GT angular-differential cross sections at 7.5 and 25 keV/u are presented, together with the measurements reported in [12]. To compare with the experimental data, we tried to model the experimental conditions by convoluting our raw data by a Gaussian function which corresponds to the experimental resolution. We used the full width at half maximum (FWHM) equal to the experimental resolution: FWHM = 0.18 and 0.1 mrad [12,31] are used for impact energies 7.5 and 25 keV/u, respectively. Our convoluted cross sections are also presented in Fig. 5 where our calculated GT angular-differential cross sections for both 7.5 and 25 keV/u are slightly larger than the experimental measurements. This is due to the fact that the absolute values of the experimental data were determined by normalization with the SET cross sections from Ref. [28], which are slightly smaller than our calculated total SET cross sections for $E > 3$ keV/u.

Except for that scaling factor, an excellent agreement can be found in Fig. 5(b) between the present convoluted results and the experimental measurements at impact energy 25 keV/u.

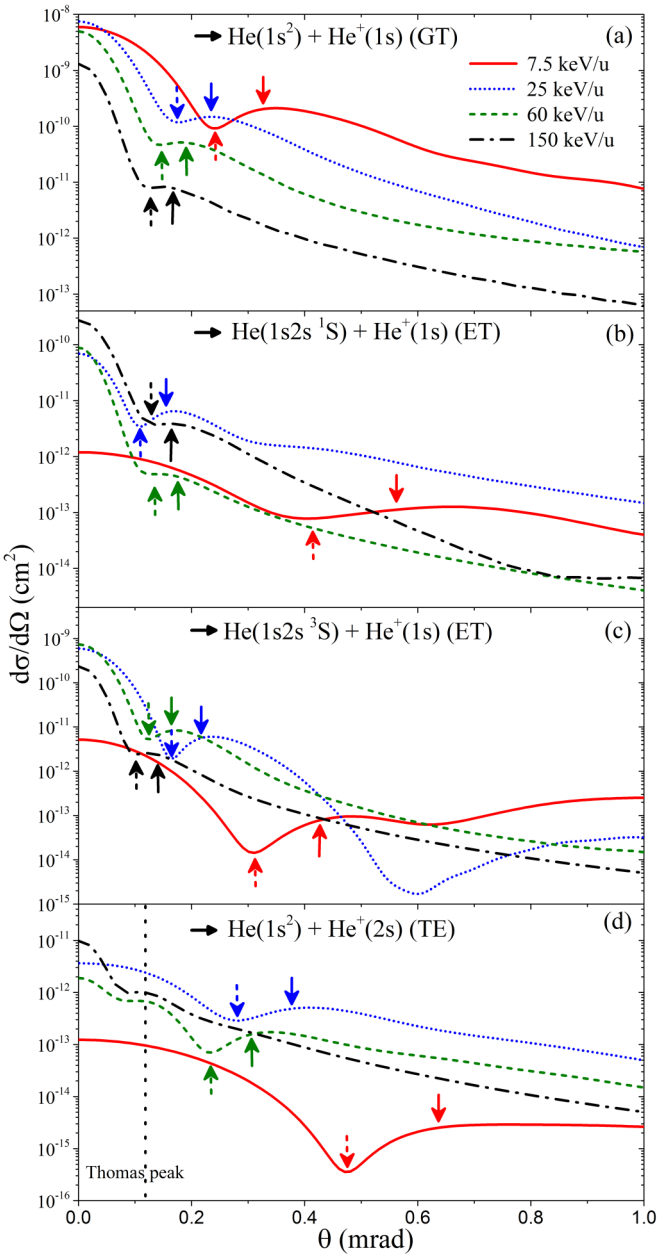

FIG. 6. Angular-differential cross sections of GT and ET to $He(1s2s\ ^1S$ and $^3S)$ excited states and TE to $He^{+}(2s) + He(1s^2)$ as functions of scattering angle for impact energies 7.5, 25, 60, and 150 keV/u. The dash-line arrows show the positions of the first minimum in our angular-differential cross sections; the solid-line arrows show the positions of the first bright fringe calculated by the Fraunhofer-type diffraction model; the vertical dot-line in (d) shows the position of the Thomas peak.

For impact energy 7.5 keV/u, our calculated GT angular-differential cross sections with convolution are also in good agreement with experimental measurements of [12], except for a small shift of the positions of maximum and minimum. This may be due to that the FWHM (∼0.18 mrad) of the Gaussian function used in our convolution was evaluated as being too large since the experimental cross sections lie between our convoluted and nonconvoluted cross sections. Note that

TABLE I. Positions of the first minimum and maximum in the angular-differential cross sections as well as the effective aperture radius ρ_{FD} and the positions of the first bright fringe calculated by the Fraunhofer-type diffraction model.

Process	Impact energy (keV/u)	1st minimum (mrad)	ρ_{FD} (a.u.)	1st maximum (mrad)	1st bright fringe (mrad)
GT	7.5	0.24	4.0	0.33	0.32
	25	0.17	3.1	0.23	0.23
	60	0.14	2.4	0.18	0.19
	150	0.13	1.7	0.15	0.17
ET to He($1s2s\ ^1S$)	7.5	0.41	2.3	0.65	0.56
	25	0.11	4.8	0.17	0.15
	60	0.13	2.6	0.17	0.18
	150	0.12	1.8	0.15	0.16
ET to He($1s2s\ ^3S$)	7.5	0.31	3.1	0.48	0.42
	25	0.16	3.3	0.23	0.21
	60	0.12	2.8	0.17	0.16
	150	0.10	2.1	0.13	0.14
TE to $He^+(2s)$	7.5	0.47	2.0	0.66	0.64
	25	0.28	1.9	0.40	0.37
	60	0.23	1.5	0.33	0.30
	150	0.09	2.4	0.12	0.12

we have also calculated the GT angular-differential cross sections of $^3He^+ + {}^4He$ collisions for 60 and 150 keV/u impact energies to compare with experimental results of Schöffler *et al.* [11]; our results and experimental results are in good agreement for both impact energies. (See Figs. 9 and 10 in the Appendix).

We now investigate the angular-differential cross sections for other electron transfer processes and larger collision energies. Figure 6 shows our cross sections for the processes GT and ET to He($1s2s\ ^1S$ and ^3S) excited states and TE to $He^+(2s)$ excited state for impact energies 7.5, 25, 60, and 150 keV/u. One can observe in Fig. 6 that the cross sections for all these processes display a similar oscillatory structure, with a first pronounced minimum followed by shallow ones in some cases. This behavior has been observed in the past [12,32–37], the oscillatory structures being interpreted by Fraunhofer-type diffraction: the angular-differential cross sections present a minimum and then a maximum like the diffraction pattern in optics, with the first dark and bright fringes located at $0.61\lambda/\rho$ and $0.819\lambda/\rho$ respectively, in the case of a circular aperture of radius ρ and of a radiation of wavelength λ, see [38].

In the following, we check the validity of this interpretation for all processes and energies considered in this work. First, let us apply it to the GT angular-differential cross sections presented in Fig. 6(a). The positions of the first minimum θ_{min}, marked as dash-line arrows, are determined directly from the calculated cross sections. From these minimum, an effective "aperture" radius ρ_{FD} is obtained so that the position of the first expected Fraunhofer bright fringe θ_{bright} is evaluated (see above). In Table I, the values of our calculated effective aperture radius and the positions of first bright fringe are shown, the latter are also marked in Fig. 6(a) as solid-line arrows. It can be seen in Table I and in Fig. 6(a) that for the four energies under consideration, the positions of the first maximum in our cross sections agree well with the predicted positions stemming from the Fraunhofer-type diffraction model. To compare our calculated effective aperture radius with the corresponding effective impact parameter range, the probabilities of the GT process as a function of impact parameter are shown in Fig. 7 for impact energies 7.5, 25, 60, and 150 keV/u. Our calculated effective aperture radii for the corresponding impact energies are denoted as arrows in the same figure. It is found that the probabilities of all these impact energies are negligibly small beyond the corresponding positions of the arrow. The effective impact parameter range is therefore in good agreement with the effective aperture radius. This tends to indicate that the oscillatory structure appearing in the GT angular-differential cross sections originates mainly from Fraunhofer-type diffraction.

We now apply the same analysis on the processes of ET to He($1s2s\ ^1S$ and ^3S) excited states and TE to $He^+(2s)$ excited state. The results are presented in Figs. 6(b)–6(d)

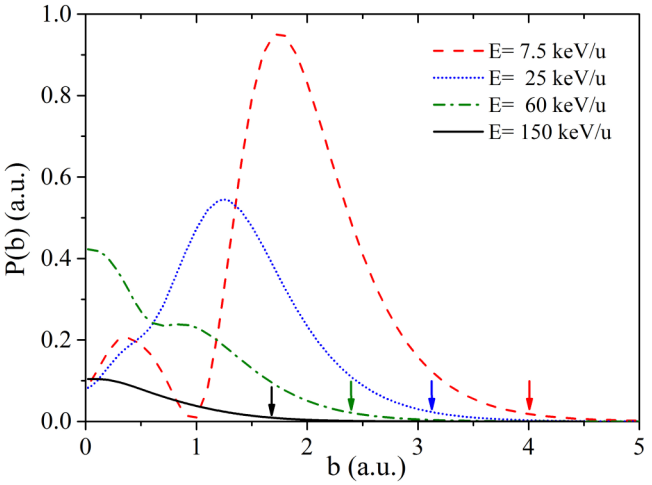

FIG. 7. Transition probabilities of the GT process as functions of impact parameters and for four different impact energies. The arrows mark the positions of the effective aperture radius calculated by the Fraunhofer-type diffraction model, see Table I.

and in Table I. The overall satisfactory agreement between the positions of the arrow and the first maximum in our calculated angular-differential cross sections suggests that the oscillatory structure observed for the ET and TE processes also originates from Fraunhofer-type diffraction. Note that we have also compared our calculated effective aperture radius with the corresponding effective impact parameter range for these processes and a satisfactory agreement was found (not shown).

However, for the TE angular-differential cross sections at 60 keV/u impact energy, one can observe an extra minimum at angle $\theta \approx 0.09$ mrad before the minimum marked as dash-line arrow in Fig. 6(d). This small angle minimum gives the aperture radius to be 3.8 a.u., while the corresponding probability is already negligibly small beyond $b \approx 1.5$ a.u.. This means that the first minimum and maximum are not stemming from Fraunhofer-type diffraction. In contrast, from the second minimum at angle $\theta \approx 0.23$ mrad marked as the dash-line arrow in Fig. 6(d), the aperture radius is determined to be 1.5 a.u., which is in good agreement with the corresponding effective probability range; the predicted first bright Fraunhofer fringe is also in agreement with the second maximum in our cross sections (see Table I). In fact, at the two highest impact energies, electron transfer is more likely dominated by the Thomas process [39–42], where the Thomas peak is located at $\theta = \sqrt{3}m/2M$ (here m and M are the masses of the electron and projectile, respectively). For the present collision system, $\theta_{\text{Thomas}} = 0.119$ mrad, which is also denoted as a vertical dot-line in Fig. 6(d). An excellent agreement can be found between the vertical dot-line and the first maximum in angular-differential cross sections for impact energy 60 keV/u. This means that the first maximum observed in the TE angular-differential cross sections of impact energy 60 keV/u is the Thomas peak, while the second one originates from Fraunhofer-type diffraction. For $E = 150$ keV/u, the first minimum is observed at angle $\theta \approx 0.09$ mrad, from which the aperture radius is determined to be 2.4 a.u. It turns out that the effective impact parameter range for this process at this energy is also around 2.4 a.u. This gives the first bright fringe of Fraunhofer-type diffraction at 0.12 mrad, which agrees well with the position of the first maximum in the angular-differential cross sections (see Table I) and also lies at the Thomas peak position. Therefore, we may conclude that the structure observed for this process at 150 keV/u stems from the overlap between Thomas mechanism and diffraction, while at 60 keV/u the two effects are separated.

Note finally that for some of considered cross sections one can observe a second minimum which does not follow Fraunhofer diffraction prediction: for instance, for ET to He($1s2s\ ^3S$) excited states [Fig. 6(c)] at 25 keV/u, a second minimum is located at 0.6 mrad while Fraunhofer theory predicts $\theta = 1.116\lambda/\rho \approx 0.29$ mrad. Furthermore, a second minimum and maximum are not observed in most cases. We attribute this fact to the limit of the Fraunhofer-type model: in particular, (i) the interaction region where electron transfer occurs is not a clean circular aperture and (ii) at larger scattering angles the contributions of hard (small impact parameters) collisions become dominant with important internuclear repulsive interaction, which washes out the diffraction pattern.

IV. CONCLUSION

In this paper, we have investigated electron transfer processes occurring in the course of $He^+ + He$ collisions by using a three-electron SCAOCC approach. First, total and state-selective cross sections have been calculated in a wide energy region from 1 to 225 keV/u and compared with available experimental and theoretical results: a very good agreement with the most recent and detailed experiments is observed. Comparisons of our results with other theoretical calculations further demonstrate the importance of a nonperturbative approach and of the electronic correlation. Moreover, we have shown that the transfer-excitation cross sections exhibit a prominent oscillatory energy dependence structure which was attributed to a strong competition between transfer-excitation and projectile-excitation processes.

Second, we have calculated angular-differential cross sections of ground-state transfer, transfer to excited state, and transfer excitation. The ground-state transfer angular-differential cross sections are in excellent agreement with experimental data of [12] for both impact energies 7.5 and 25 keV/u.

Finally, the oscillatory structures observed in the ground-state transfer, transfer to excited state, and transfer-excitation angular-differential cross sections have been interpreted by Fraunhofer-type diffraction, which seems to be valid for all processes and energies considered in this work. The Thomas peak has also been observed in the transfer-excitation angular-differential cross sections for higher impact energies 60 and 150 keV/u. In the latter case, the Thomas peak overlaps with the Fraunhofer-type maximum.

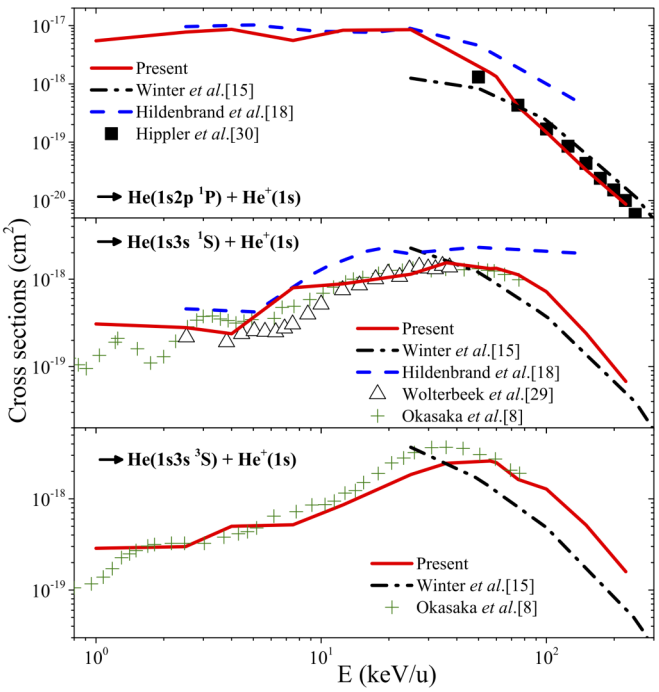

FIG. 8. Present cross sections for electron transfer to He($1s2p\ ^1P$ and ^3P, $1s3s\ ^1S$ and ^3S) excited states, compared with available theoretical [15,18] and experimental [8,29,30] results.

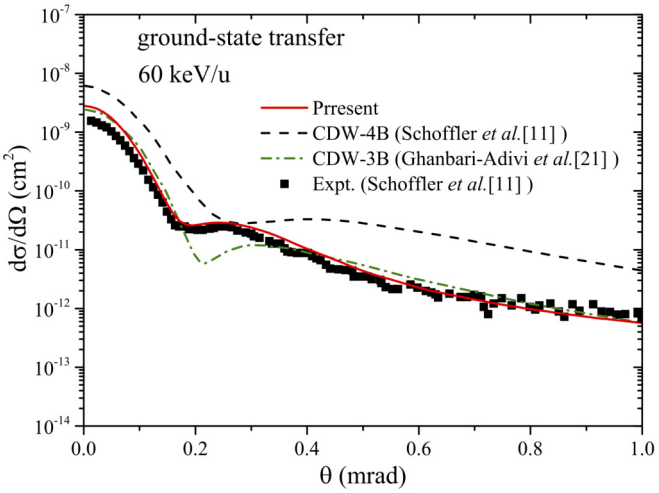

FIG. 9. GT angular-differential cross sections as a function of scattering angle at impact energy 60 keV/u. Red solid line: present calculations; black dash line: theoretical results of Schöffler *et al.* [11]; green dash-dot line: theoretical results of Ghanbari-Adivi *et al.* [21]; black solid squre: experimental results of Schöffler *et al.* [11].

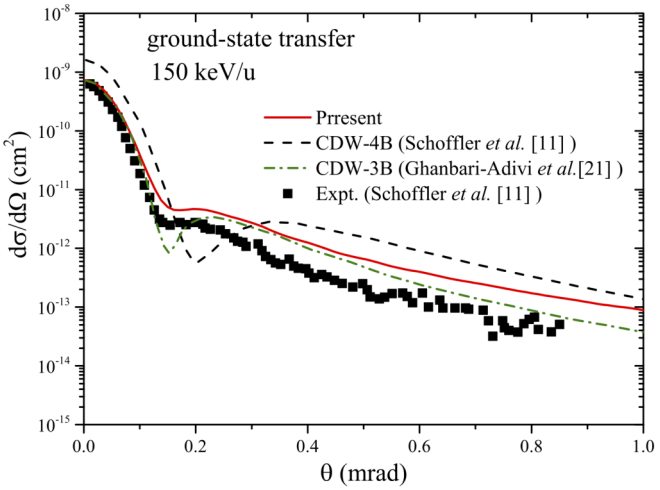

FIG. 10. Same as Fig. 9, but for 150 keV/u.

ACKNOWLEDGMENTS

The authors thank D. L. Guo and X. Ma for useful discussions. J.W.G. is supported by a China Scholarship Council (CSC) scholarship, within a CSC-SU program. Y.W. acknowledges the support of the a National Key Research and Development Program of China under Grants No. 2017YFA0403200 and No. 2017YFA0402300 and the National Natural Science Foundation of China (Grants No. 11474032 and No. 11534011U1530261). This work was partly supported by LABEX Plas@par (France) under Grant No. ANR-11-IDEX-0004-02.

APPENDIX: ADDITIONAL CALCULATIONS

The validity of our results for electron transfer to He($1s2s\ ^1S$ and ^3S) excited states and transfer and target excitation to $He^+(2s)$ excited state is also supported by the comparison with experiments concerning electron transfer to higher He($1s2p\ ^1P$, $1s3s\ ^1S$ and ^3S) excited states. As shown in Fig. 8, Our results are in excellent agreement with the experimental results of [8,29,30] in the overlapping energy regions.

We have also calculated the GT angular-differential cross sections of $^3He^+ + {}^4He$ collisions for 60 and 150 keV/u impact energies, which are in good agreement with experimental results [11] for both impact energies (see Figs. 9 and 10).

[1] C. F. Barnett and P. M. Stier, Phys. Rev. **109**, 385 (1958).
[2] W. N. Shelton and P. A. Stoycheff, Phys. Rev. A **3**, 613 (1971).
[3] V. Pol, W. Kauppila, and J. T. Park, Phys. Rev. A **8**, 2990 (1973).
[4] R. Hegerberg, T. Stefansson, and M. T. Elford, J. Phys. B **11**, 133 (1978).
[5] E. A. Hinds and R. Novick, J. Phys. B **11**, 2201 (1978).
[6] N. V. de Castro Faria, F. L. Freire, and A. G. de Pinho, Phys. Rev. A **37**, 280 (1988).
[7] R. D. DuBois and S. T. Manson, Phys. Rev. A **42**, 1222 (1990).
[8] R. Okasaka, K. Kawabe, S. Kawamoto, M. Tani, H. Kuma, T. Iwai, K. Mita, and A. Iwamae, Phys. Rev. A **49**, 246 (1994).
[9] J. L. Forest, J. A. Tanis, S. M. Ferguson, R. R. Haar, K. Lifrieri, and V. L. Plano, Phys. Rev. A **52**, 350 (1995).
[10] H. Atan, W. Steckelmacher, and M. W. Lucas, J. Phys. B **24**, 2559 (1999).
[11] M. S. Schöffler, J. Titze, L. P. H. Schmidt, T. Jahnke, N. Neumann, O. Jagutzki, H. Schmidt-Böcking, R. Dörner, and I. Mančev, Phys. Rev. A **79**, 064701 (2009).
[12] D. L. Guo, X. Ma, R. T. Zhang, S. F. Zhang, X. L. Zhu, W. T. Feng, Y. Gao, B. Hai, M. Zhang, H. B. Wang, and Z. K. Huang, Phys. Rev. A **95**, 012707 (2017).
[13] M. Barat, D. Dhuicq, R. Francois, R. McCarroll, R. D. Piacentini, and A. Salin, J. Phys. B **5**, 1343 (1972).
[14] E. Ghanbari-Adivi and H. Ghavaminia, Chin. Phys. B **24**, 033401 (2015).
[15] T. G. Winter and C. C. Lin, Phys. Rev. A **12**, 434 (1975).
[16] W. Lichten, Phys. Rev. **131**, 229 (1963).
[17] D. P. Sural, S. C. Mukherjee, and N. C. Sil, Phys. Rev. **164**, 156 (1967).
[18] R. Hildenbrand, N. Grun, and W. Scheid, J. Phys. B **28**, 4781 (1999).
[19] I. Mančev, Phys. Rev. A **75**, 052716 (2007).
[20] M. Baxter, T. Kirchner, and E. Engel, Phys. Rev. A **96**, 032708 (2017).
[21] E. Ghanbari-Adivi and H. Ghavaminia, Eur. Phys. J. D **66**, 350 (2012).
[22] N. Sisourat, I. Pilskog, and A. Dubois, Phys. Rev. A **84**, 052722 (2011).
[23] G. Labaigt, A. Jorge, C. Illescas, K. Béroff, A. Dubois, B. Pons, and M. Chabot, J. Phys. B **48**, 075201 (2015).
[24] J. W. Gao, Y. Wu, N. Sisourat, J. G. Wang, and A. Dubois, Phys. Rev. A **96**, 052703 (2017).

[25] L. Shampine and M. Gordon, *Computer Solution of Ordinary Differential Equations: The Initial Value Problem* (Freeman, San Francisco, CA, 1975).
[26] A. Dubois, S. E. Nielsen, and J. P. Hansen, J. Phys. B **26**, 705 (1993).
[27] R. Piacentini and A. Salin, Comput. Phys. Commun. **13**, 57 (1977).
[28] C. F. Barnett, H. T. Hunter, M. I. Fitzpatrick, I. Alvarez, C. Cisneros, and R. A. Phaneuf, *Atomic Data for Fusion. Volume 1: Collisions of H, H2, He and Li Atoms and Ions with Atoms and Molecules* (Oak Ridge National Laboratory, Oak Ridge, US, 1990).
[29] L. Wolterbeek Muller and F. J. De Heer, Physica **48**, 345 (1970).
[30] R. Hippler, K. H. Schartner, and H. F. Beyer, J. Phys. B **11**, L337 (1978).
[31] Private communications with the authors of Ref. [12].
[32] M. van der Poel, C. V. Nielsen, M. A. Gearba, and N. Andersen, Phys. Rev. Lett. **87**, 123201 (2001).
[33] M. van der Poel, C. V. Nielsen, M. Rybaltover, S. E. Nielsen, M. Machholm, and N. Andersen, J. Phys. B **35**, 4491 (2002).
[34] Q. Wang, X. Ma, X. L. Zhu, and S. F. Zhang, J. Phys. B **45**, 025202 (2011).
[35] H. Agueny, Phys. Rev. A **92**, 012702 (2015).
[36] M. Gudmundsson, D. Fischer, N. Haag, H. A. B. Johansson, D. Misra, P. Reinhed, H. Schmidt-Böcking, R. Schuch, M. Schöffler, K. Støchkel, H. T. Schmidt, and H. Cederquist, J. Phys. B **43**, 185209 (2010).
[37] S. E. Nielsen, T. H. Rod, J. Salgado, D. Dowek, J. C. Houver, J. W. Thomsen, and N. Andersen, J. Phys. B **37**, 2119 (2004).
[38] M. Born and E. Wolf, *Principles of Optics: Electromagnetic Theory of Propagation, Interference and Diffraction of Light*, 7th ed. (Cambridge University, Cambridge, England, 2003).
[39] L. H. Thomas, Proc. R. Soc. London, Ser. A **114**, 561 (1927).
[40] E. Horsdal-Pedersen, C. L. Cocke, and M. Stockli, Phys. Rev. Lett. **50**, 1910 (1983).
[41] D. Fischer, K. Støchkel, H. Cederquist, H. Zettergren, P. Reinhed, R. Schuch, A. Källberg, A. Simonsson, and H. T. Schmidt, Phys. Rev. A **73**, 052713 (2006).
[42] V. Mergel, R. Dörner, M. Achler, K. Khayyat, S. Lencinas, J. Euler, O. Jagutzki, S. Nuttgens, M. Unverzagt, L. Spielberger, W. Wu, R. Ali, J. Ullrich, H. Cederquist, A. Salin, C. J. Wood, R. E. Olson, D. Belkic, C. L. Cocke, and H. Schmidt-Bocking, Phys. Rev. Lett. **79**, 387 (1997).